Magnetic coupling between Sm^{3+} and the canted spin in an antiferromagnetic SmFeO_{3} single crystal

L. G. Marshall, J.-G. Cheng, J.-S. Zhou, J. B. Goodenough, J.-Q. Yan, and D. G. Mandrus

Phys. Rev. B **86**, 064417 — Published 13 August 2012

DOI: 10.1103/PhysRevB.86.064417

The magnetic coupling between Sm^{3+} and the canted spin in an antiferromagnetic $SmFeO_3$ single crystal

L. G. Marshall [1], J.-G. Cheng [1], J.-S. Zhou [1*], J. B. Goodenough [1], J.-Q. Yan [2,3], and D. G. Mandrus [2,3]

[1] Materials Science and Engineering Program/Mechanical Engineering, The University of Texas at Austin, Austin, TX 78712, USA
[2] Materials Science and Technology Division, Oak Ridge National Laboratory, Oak Ridge, TN 37831, USA
[3] Department of Materials and Engineering, The University of Tennessee, Knoxville, TN 37996 USA

Abstract

The perovskite $SmFeO_3$ exhibits type-G AF ordering at $T_N \approx 670$ K and an easy axis rotation transition at $T_{SR} \approx 480$ K. Owing to the peculiar site anisotropy of rare-earth Sm^{3+}, the moment on Sm^{3+} is oriented antiparallel to the canted spin from the Fe^{3+} sublattice along the *a* axis at $T < T_{SR}$. Development of the magnetic moment on Sm^{3+} as temperature decreases makes it possible to balance the two magnetic moments at T_{comp}. Application of a moderate external magnetic field along the *a* axis can trigger an abrupt reversal of the moment on Sm^{3+} and the canted spin relative to the external field at a temperature around T_{comp}. We report here a study of the field-induced magnetic-moment reversal in a single crystal $SmFeO_3$ by measuring the magnetization and specific heat with the external field along different crystallographic axes.

Although the physical properties of the perovskite oxides RMO_3 (R = rare earth, M = transition metal) are dominated by the M-ion array, the interaction between the rare-earth R and M sublattices can induce unusual phenomena such as spin rotation transitions on both sublattices and charge transfers. For example, the sharp metal-insulator transition in the $Pr_{0.5}Ca_{0.5}CoO_3$ perovskite, which was previously attributed to a spin-state transition of Co ions, [1] was recently clarified as being due to a real charge transfer between Pr and Co ions, i.e. 0.5 Pr^{3+} + $Co^{3.5+}$ → 0.5 Pr^{4+} + Co^{3+}. [2, 3] Recent studies on perovskite $SmMnO_3$ [4, 5] have shown another unusual magnetic phenomenon associated with the coupling between the rare-earth Sm^{3+} and the Mn^{3+}. In this compound, the Mn^{3+}-ion sublattice exhibits the type-A antiferromagnetic order below $T_N \approx 60$ K with a weak canted-spin ferromagnetic moment along the crystallographic *c* axis of the *Pbnm* structure. Below T_N, the magnetic moment on Sm^{3+} ions is progressively oriented antiparallel to the canted-spin ferromagnet moment parallel to the *c* axis from the Mn^{3+}-ion array due to an internal exchange field H_{in} along the *c* direction. When a small magnetic field, *e.g.* 500 Oe, is applied along the *c* axis, the Sm^{3+} moment dominates the canted-spin Mn^{3+} moment below a compensation temperature $T_{comp} \approx 9$ K, leading to a negative magnetization. Moreover, applying an external magnetic field $H_{ex} \geq 1$ T along the *c* axis results in a simultaneous reversal of both the moment on Sm^{3+} and the canted spin moment from Mn^{3+} relative to the direction of the external field at temperatures $T_t^{\pm} = T_{comp} \pm \delta$; this reversal manifests as a sudden jump in the magnetic susceptibility, specific heat, and dielectric constant.[4] The thermal hysteresis loop $\Delta T = T_t^+ - T_t^-$ associated with this first-order transition depends sensitively on the magnitude of H_{ex}, *i.e.* the larger H_{ex}, the smaller ΔT. This unusual magnetic moment reversal is due to the peculiar site anisotropy on Sm^{3+} that places the rare-earth moment antiparallel to the exchange field from the Mn^{3+} array. This type of temperature-induced magnetization reversal has also been observed in some other RMO_3 antiferromagnetic materials. [6-10] In comparison, the moment on Nd^{3+} in the perovskite $NdMnO_3$ is along the direction of the canted-spin from Mn^{3+}; [11, 12] while the moment on Pr^{3+} is perpendicular to the canted spin on Mn^{3+} in the perovskite $PrMnO_3$. [12] In order to verify whether all the observations made on the $RMnO_3$ crystals are applicable only to the type-A AF magnets or are universal for all types of AF magnets with a canted spin structure, we have carried out a similar study on a

perovskite $SmFeO_3$ crystal. In this compound, the Fe^{3+} sublattice exhibits a type-G antiferromagnetic order at a $T_N \approx 670$ K. [13] In contrast to $SmMnO_3$, the spin direction on Fe^{3+} in $SmFeO_3$ changes from the *b* axis at $T < T_N$ to the *c* axis at $T < T_{SR} = 480$ K, [14] which makes the canted moment along the *a* axis at $T < T_{SR}$. It is also reported that the magnetization M_a for the magnetic field (H = 0.01 T) along the *a* axis crosses zero at $T \approx 5$ K, [14, 15] which may signal a magnetic moment compensation between the moments on Sm^{3+} and the canted spin on Fe^{3+} similar to that between the moment on Sm^{3+} and the canted spin on Mn^{3+} in $SmMnO_3$. Therefore, we have explored the possible moment reversal at higher magnetic fields. In this paper, we report measurements of the magnetization and specific heat on a single crystal of $SmFeO_3$ under different magnetic fields applied along all principal crystallographic axes. Nearly identical observations made on $SmFeO_3$ and on $SmMnO_3$ give rise to a simple rule that the moments on Sm^{3+} are always opposite to the canted-spin moment of the MO_3 array in the orthorhombic perovskites.

The $SmFeO_3$ single crystal used in the present study was grown in an infrared-heating image furnace (NEC SC-M35HD). The starting ceramic rods of $SmFeO_3$ were the product of a reaction between Sm_2O_3 (Alfa Aesar, 99.9%) and Fe_2O_3 (Alfa Aesar, 99.998%) in a 1:1 ratio. The crystals were grown by the floating zone method [16] in a flow of air. The phase purity was confirmed by powder X-ray diffraction. Laue back reflection was used to check the crystal quality and to orient the crystals along the three principal axes with an error less than 1°. Measurements of the magnetization have been carried out in a commercial Superconducting Quantum Interference Device (SQUID) magnetometer (Quantum Design). The specific heat was measured in different applied magnetic fields with a Physical Property Measurement System (Quantum Design) by using the two-τ relaxation method at temperatures from 2 to 20 K and under different magnetic fields up to 10 T. The background from the sample holder and the Apiezon N grease was recorded in different magnetic fields and was subtracted from the total specific heat.

Fig. 1 shows the temperature dependence of the magnetization M(T)/H of the $SmFeO_3$ crystal oriented along the three principal axes with H = 0.1 T and in the temperature

range 2-300 K, which is far below the long-range antiferromagentic ordering temperature $T_N \approx 670$ K and the spin-reorientation temperature $T_{SR} = 480$ K. Consistent with the fact that the magnetic easy axis of $SmFeO_3$ changes from the *b* axis to the *c* axis and the canting direction is along the *a* axis below T_{SR}, the $M_a(T)$ is nearly one order of magnitude higher than $M_b(T)$ and $M_c(T)$. The main features of the M(T) curves occur at low temperatures where the moment on Sm^{3+} starts to align with the exchange field from the Fe^{3+} sublattice. The influence of Sm^{3+} moments on the overall magnetization along the *a* axis shows up at $T \approx 140$ K. The net moment experiences a crossover from a dominant canted spin from the Fe^{3+} sublattice to a dominant Sm^{3+} moment on cooling through $T_{comp} = 3.7$ K. The observed M_a in our crystal grown with the floating-zone method is almost identical to that measured by Lee *et al.*; [14] their crystal was grown with the flux method. We noticed that the $M_b(T)$ curve in Fig. 1 also crosses zero at $T \approx 3.7$ K and resembles the same feature as that of $\chi_a(T)$. The most likely reason for this behavior is the twinning formed during crystal growth. As a matter of fact, twinning on the *ab* plane has been widely observed in the orthorhombic *Pbnm* perovskite oxides in which there is a phase transition to the phase with higher symmetry, i.e. the rhombohedral phase R-3c or the tetragonal phase I4/mcm at high temperatures. The twinning is difficult to detect with Laue back reflection, especially in the case of $a \approx b$. However, this kind of twinning should not affect the magnetization along the *c* axis and this is indeed confirmed by the $M_c(T)$ shown in Fig. 1. A totally detwinned $SmFeO_3$ crystal requires a slow cooling process under uniaxial pressure through the *Pbnm*-to-*R3-c* phase transition. The phase transition temperature remains unknown to us. The crystals used in this study are not totally detwinned. In the following, we will focus on measurements of the $SmFeO_3$ crystal with magnetic field oriented along the *a* axis where the highest magnetization has been detected.

The $M_a(T)$ curves of the $SmFeO_3$ crystal shown in Fig. 2 were measured with thermal cycling between 2 and 10 K under various magnetic fields H_{ex} up to 5 T. At $H_{ex} > 0.2$ T, an abrupt change of $M_a(T)$ has been observed on cooling at $T_t = T_{comp} - \delta$ and warming at $T_t' = T_{comp} + \delta'$, resulting in an asymmetric butterfly-shaped hysteresis loop. The field dependence of T_t and T_t' are shown in the inset of Fig. 2. With increasing H_{ex}, the

thermal hysteresis loop $\Delta T = T_t - T_t'$ becomes smaller and the loop becomes less obvious at $H_{ex} > 1.5$ T. The magnetization M no longer crosses zero for $H_{ex} > 0.3$ T. These features observed for M_a in the present $SmFeO_3$ are very similar to those of the M_c found in a $SmMnO_3$ crystal with H_{ex} applied along the *c* axis. [4] From these observations and their comparison with those for $SmMnO_3$, we conclude that applying an external field $H_{ex} > 0.2$ T along the spin canting direction leads to a simultaneous flipping of both the Sm^{3+} moments and the canted-spin magnetization of the FeO_3 array.

As demonstrated in the case of a $SmMnO_3$ single crystal, [4] the magnetic-field-induced moment reversal can be verified by low-temperature specific-heat measurements. The ground state of the free Sm^{3+} ion, $^6H_{5/2}$, is split into three Kramer's doublets in the crystal field. According to the result of inelastic neutron scattering on the isostructural $SmNiO_3$, these three doublets are separated by 220 K and 450 K, respectively. [17] The internal exchange field on the Sm^{3+} site further splits the lowest Kramer's doublet by $\Delta E = \Delta_g/k_B$, where k_B is the Boltzmann constant. This splitting is reflected in the specific heat C(T) measurement by a Schottky anomaly at $T < 20$ K. Fig. 3 shows the specific heat C(T) of a $SmFeO_3$ crystal measured upon both heating and cooling in the temperature range 2-20 K and under various magnetic fields up to 10 T applied along the *a* axis. The C(T) at H = 0 exhibits a dramatic increase down to 2 K relative to that of $LaCrO_3$ due to the Schottky contribution of Sm^{3+}; but a complete profile of the Schottky contribution to C(T) is not fully developed at 2K, the lowest temperature in this study, since the gap $\Delta_g/k_B(H = 0)$ is small. There is no observable difference between the curves during heating up and cooling down. Although the spin reversal can be clearly seen in the magnetization measurement of Fig. 1 with H_{ex} as large as 1 T, the magnetic field is still too small to make an obvious change on the Schottky anomaly to C(T), which is dominated by a huge internal exchange field $H_{in} \sim 11$ T as determined by the following curve fitting. With increasing applied magnetic field, the Schottky anomaly moves to higher temperatures, which allows us to see the more complete profile of C(T) from the Schottky anomaly. Moreover, in accordance with the abrupt change at T_t in the $M_a(T)$ data, an abrupt drop/jump of C(T) was observed at T_t and T_t' during heating/cooling, which can be seen

more clearly in the inset of Fig. 3. However, these anomalies are less pronounced than those observed in $SmMnO_3$.[4]

Fitting the C(T) under different magnetic fields to the formula of the Schottky anomaly, we can obtain the quantitative information on such parameters as the gap $\Delta_g/k_B(H)$, the internal exchange field H_{in}, the effective moment of the Sm^{3+} ions, as well as the relative orientation of H_{in} with respect to the H_{ex}. We have fitted the C(T) data of $SmFeO_3$ in Fig. 3 by taking into account three contributions, *e.g.* the lattice and spin wave $C_{lat} + C_{sw}$, the Schottky contribution C_{Sch}, and the crystal-field contribution C_{CF}. Both the $C_{lat} + C_{sw}$ and C_{CF} terms do not contribute to the low-temperature enhancement of C(T). The C(T) of isostructural $LaCrO_3$ was used to represent the $C_{lat} + C_{sw}$, while the crystal-field splitting of Sm^{3+} in $SmNiO_3$ was used to obtain the C_{CF}, [17] see Ref. 4 for details on how to decompose contributions from C_{lat}, C_{sw}, and C_{CF}. The Schottky contribution C_{Sch} is expressed as

$$C_{Sch} = R(\Delta_g / k_B T)^2 \exp(\Delta_g / k_B T) / [1 + \exp(\Delta_g / k_B T)]^2 \qquad (1)$$

where Δ_g/k_B is the splitting of the ground Kramer's doublet, k_B is the Boltzmann constant, and R is the ideal gas constant. For $H_{ex} > 0.3$ T, the external field triggers the moment reversal. In this case, the canting angle and therefore the exchange field at Sm^{3+} varies depending on whether the canted spin direction is parallel or antiparallel to the external field. The canting direction becomes antiparallel to the H_{ex} at $T < T_t$ and parallel at $T > T_t$ as illustrated in Fig. 4. The canting angle and therefore the exchange field at the Sm^{3+} site depends on the configuration between the canted spin and the external magnetic field. The abrupt change of C(T) on crossing T_t truly reflects a discontinuous change of the gap in the Schottky formula. Therefore, we have carried out the fitting procedure separately for $T < T_t$ and $T > T_t$ with two different energy gaps Δ_g/k_B. As shown in Fig. 5, the fitting curves for each field can excellently reproduce the experimental data.

The obtained Δ_g/k_B as a function of external magnetic field H_{ex} is plotted in Fig. 6. As can be seen from the plot, Δ_g/k_B for $T < T_t$ increases gradually with H_{ex}, but it does not follow a linear field dependence of $\Delta_g/k_B \propto H_{in} + H_{ex}$ for $T < T_t$ as expected for the H_{ex} applied

along the *a* axis. Similarly, for $T > T_t$, Δ_g/k_B should be proportional to $H_{in} - H_{ex}$. However, we have found that Δ_g/k_B decreases slightly and then increases with H_{ex} with a broad minimum. Although we have applied the external magnetic field H_{ex} along the *a* axis of a crystal disk, the non-linear field dependence of Δ_g/k_B indicates that the H_{ex} is actually neither parallel nor perpendicular to the internal exchange field H_{in}. Taking into account the twin formation within the *ab* plane as already observed in the χ_b, the actual situation in our C(T) measurements could be a combination of the magnetic field effect on both *a* and *b* axes. For a twined crystal, a magnetic field H_{ex} is applied within the *ab* plan and it has an angle θ relative to the *a* axis, the Δ_g/k_B will have the following field dependence:

$$\Delta_g/k_B = 2\mu_{eff}\cdot[(H_{ex}\cdot\cos\theta + H_{in})^2 + (H_{ex}\cdot\sin\theta)^2]^{1/2} \quad \text{for } T < T_t, \tag{2}$$

and

$$\Delta_g/k_B = 2\mu_{eff}\cdot[(H_{ex}\cdot\cos\theta - H_{in})^2 + (H_{ex}\cdot\sin\theta)^2]^{1/2} \text{ for } T > T_t. \tag{3}$$

As shown in Fig. 6, the $\Delta_g/k_B(H)$ for both $T< T_t$ and $T > T_t$ can be described perfectly with Equations (2, 3). The fitting parameters are given in Table 1. As can be seen, the parameters at $T < T_t$ and $T > T_t$ are highly consistent with each other, which confirms our assumption and analysis above. The obtained effective moment of Sm^{3+}, 0.33(1) μ_B, is perfectly in line with 0.36 μ_B found in $SmMnO_3$; the $H_{in} \sim 11$ T is smaller than that of ~ 18 T found in $SmMnO_3$. The angle θ indicates that most of the crystal has its *a* axis perpendicular to the external field in this measurement. The crystal cut for the magnetization measurement with the H_{ex} along the *a* axis has a smaller cross section in the *bc* plane than that used for the specific-heat measurement. Therefore, the chance to include twining domains with different orientations is significantly higher in the crystal for the specific-heat measurement. From the analysis of the specific-heat data, we further confirmed the magnetic-field-induced spin reversal of both the Sm^{3+} and the canted-spin ferromagnetic Fe^{3+} moments in $SmFeO_3$.

In conclusion, the detailed magnetic measurements and specific-heat analysis on a $SmFeO_3$ single crystal are consistent with the scenario that the rare-earth Sm^{3+} moment is antiparallel to the canted-spin ferromagnetic moment of the Fe^{3+}-ion array along the *a* axis. A moderate external magnetic field $H_{ex} > 0.2$ T applied along the *a* axis can induce

a simultaneous reversal of Sm^{3+} and the Fe^{3+} canted-spin moments relative to the external field; the magnetic moment reversal results in a sharp anomaly in both magnetization and specific heat at T_t. The analysis of the $\Delta_g/k_B(H)$ splitting on the Sm^{3+} ions further supports the above scenario. The nearly identical observations in both $SmMnO_3$ and $SmFeO_3$ indicate that the moment reversal should be a generic feature of the Sm^{3+} moment in canted-spin antiferromagentic perovskite oxides.

Acknowledgements

This work at Austin was supported by NSF (DMR 0904282, DMR 1122603) and the Robert A Welch foundation (Grant F-1066). The work at ORNL was supported by the Division of Materials Sciences and Engineering, Office of Basic Energy Sciences, U.S. Department of Energy.

∗ jszhou@mail.utexas.edu

Table 1. The fitting parameters to $\Delta_g/k_B(H)$ in Fig. 6

	$T < T_t$	$T > T_t$
μ_{eff}/Sm^{3+} (μ_B)	0.33 ± 0.01	0.30 ±0.04
H_{ex} (T)	10.7 ± 0.2	11.8 ±1.4
θ (°)	88.6 ± 1.3	75.1 ± 4.6

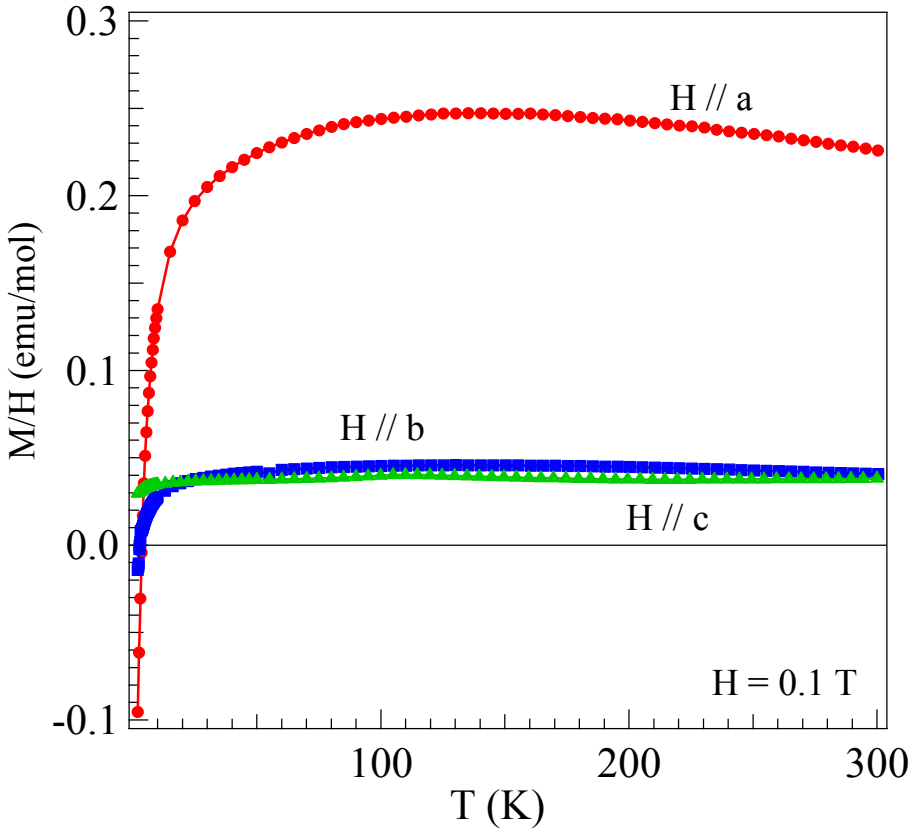

Fig. 1 (Color online) Temperature dependence of the magnetization M(T) of the $SmFeO_3$ single crystal with magnetic field H = 0.1 T applied along all three major crystallographic axes *a*, *b*, and *c*. The crystal weights for the magnetization measurements: 11.9 mg (*a* axis oriented), 7.3 mg (*b* axis oriented), 70.3 mg (*c* axis oriented).

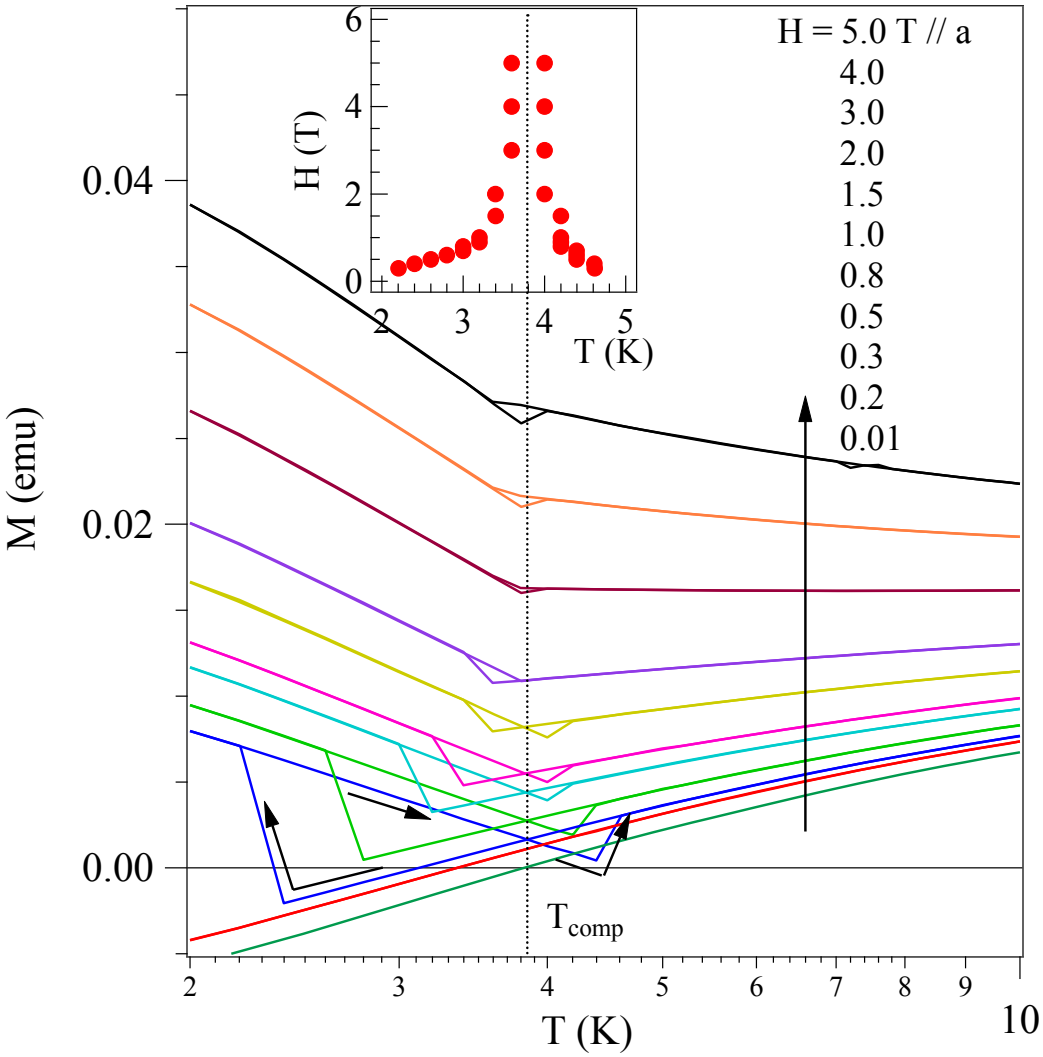

Fig. 2 (Color online) Temperature dependence of magnetization M(T) for the $SmFeO_3$ crystal with magnetic field applied along the *a* axis; the inset plot shows the transition temperatures T_t and T_t' found for different magnetic fields.

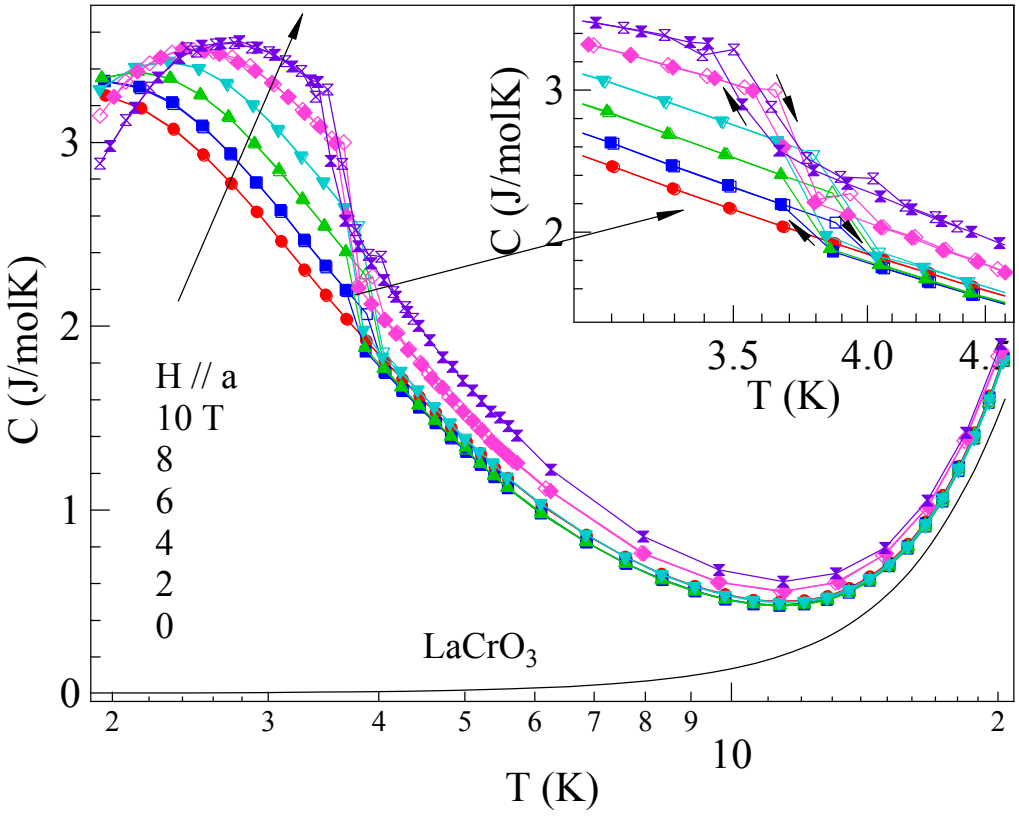

Fig. 3 (Color online) Temperature dependence of specific heat C(T) for the $SmFeO_3$ crystal with different magnetic fields applied along the *a* axis; the insert shows the C(T) near T_t. Solid symbols: C(T) measured on cooling down; open symbols: C(T) measured on heating up. A thermal hysteresis loop near T_t becomes visible at $H \geq 2$ T. The C(T) of $LaCrO_3$ is shown for comparison. The disk-shaped crystal for the specific heat measurement was oriented with the Laue back reflection in such a way that the *a* axis (and therefore the direction of external magnetic field) is normal to the crystal surface. However, the curve fitting to the magnetic field dependence of the gap Δ in Fig. 5 indicates that the external magnetic field is actually applied inside the *ab* plane and closer to the *b* axis. The crystal weight: 8.1 mg.

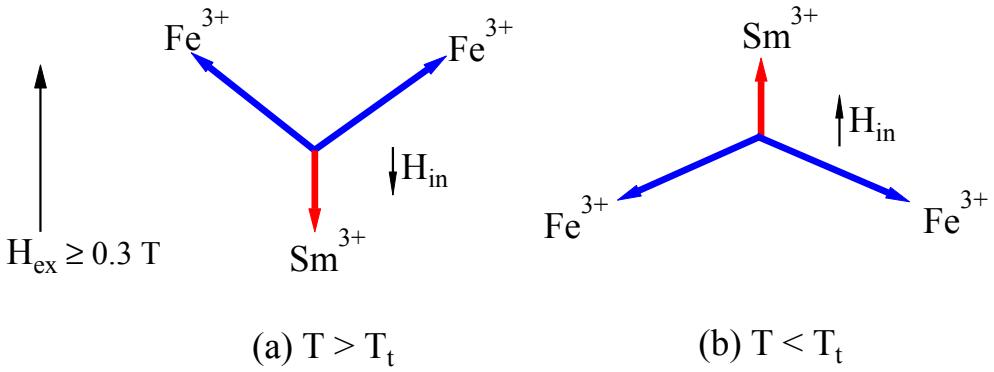

Fig. 4 (Color online) A schematic view of the relative orientation of the Sm^{3+} moment (H_{in}), the canted-spin ferromagnetic Fe^{3+} moment (// *a* axis) and the external magnetic field H_{ex} at $T < T_t$ and $T > T_t$.

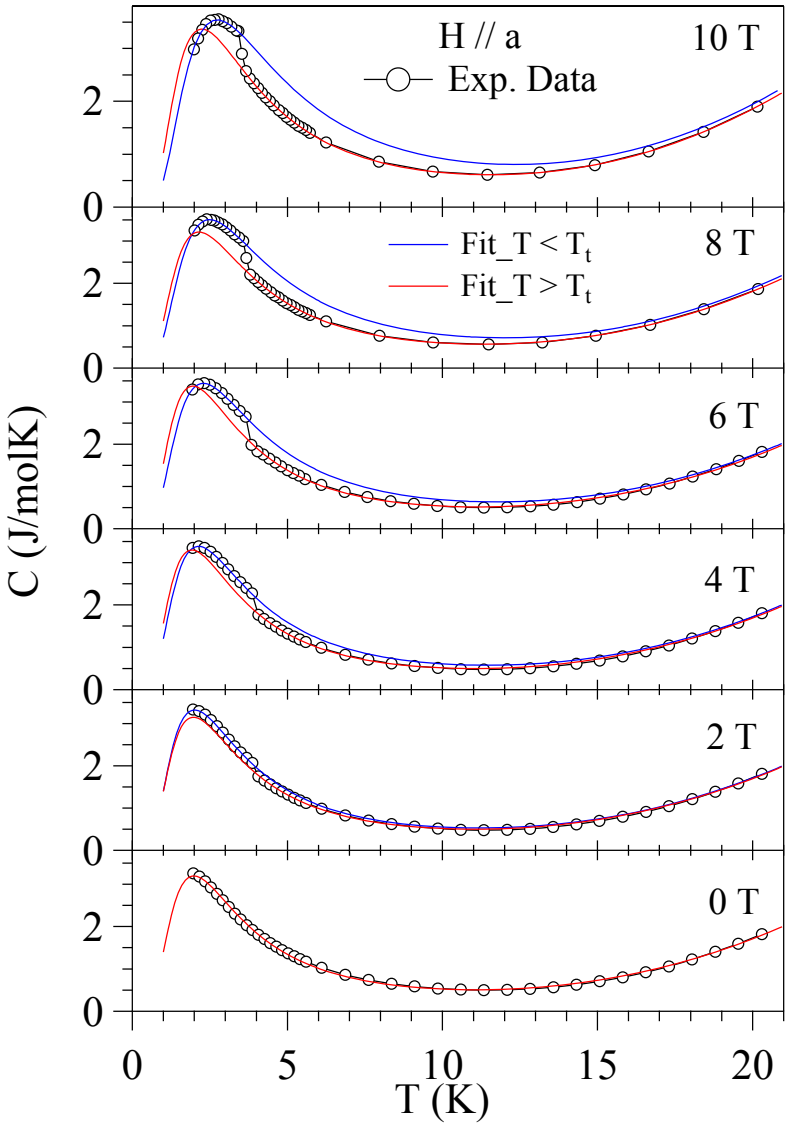

Fig. 5 (Color online) The detailed fitting curves for the C(T) for the $SmFeO_3$ crystal under different magnetic fields.

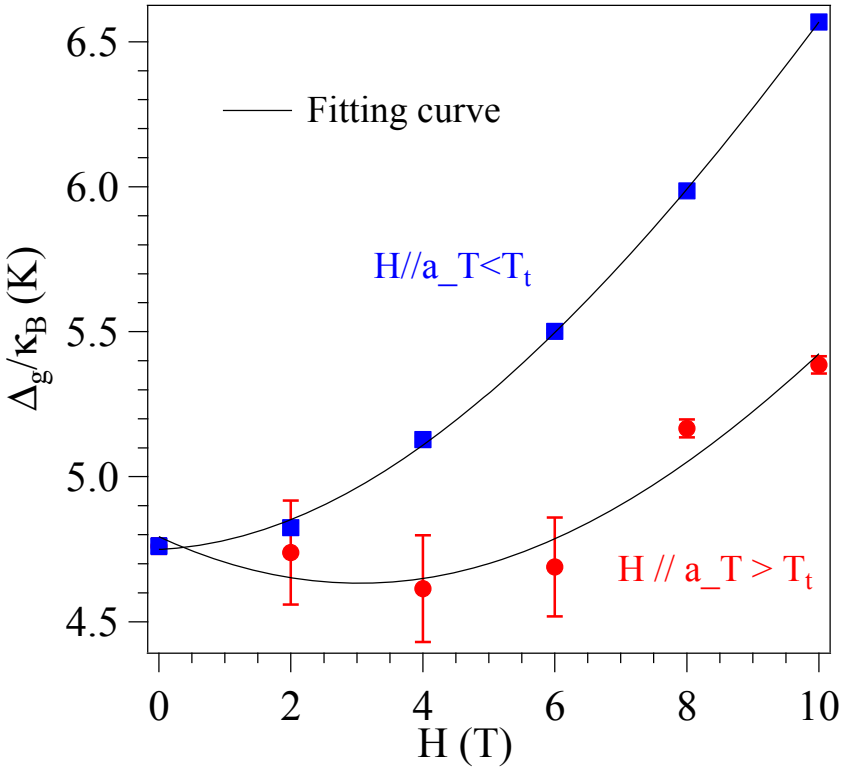

Fig. 6 (Color online) The magnetic field dependence of the energy gap Δ_g/κ_B and the curve fitting by using Eq.1 and Eq.2 in the text.

[1] S. Tsubouchi, T. Kyomen, M. Itoh, P. Ganguly, M. Oguni, Y. Shimojo, Y. Mori, and Y. Ishii, Phys. Rev. B **66**, 052418 (2002).

[2] J. Hejtmanek, E. Santava, K. Knizek, M. Marysko, Z. Firak, T. Naito, H. Sasaki, and H. Fujishiro, Phys. Rev. B **82**, 165107 (2010).

[3] J. L. Garcia-Munoz, C. Frontera, A. J. Baron-Gonzalez, S. Valencia, J. Blasco, R. Feyerherm, E. Dudzik, R. Abrudan, and F. Radu, Phys. Rev. B **84**, 045104 (2011).

[4] J.-G. Cheng, J.-S. Zhou, J. B. Goodenough, Y.T. Su, Y. Sui, and Y. Ren, Phys. Rev. B **84**, 104415 (2011).

[5] J.-S. Jung, A. Iyama, H. Nakamura, M. Mizumaki, N. Kawamura, Y. Wakabayashi, and T. Kimura, Phys. Rev. B **82**, 212403 (2010).

[6] J.B. Goodenough, H.C. Nguyen, Acad. Sci. Paris C. R. **319**, 1285 (1994).

[7] J. Mao, Y. Sui, X. Zhang, Y. Su, X. Wang, Z. Liu, Y. Wang, Z. Liu, Y. Wang, R. Zhu, Y. Wang, W. Liu, and J. Tang., Appl. Phys. Lett. **98**, 192510 (2011).

[8] H.C. Nguyen, J.B. Goodenough, Phys. Rev. B **52** 324-34 (1995).

[9] K. Yoshii, A. Nakamura, J. Solid State Chem., **155**, 447 (2000).

[10] Y. Ma, M. Guilloux-Viry, P. Barahona, O. Pena, and C. Moure, Appl. Phys. Lett., **86**, 062506 (2005).
[11] A. Munoz, J. A. Alonso, M. J. Martinez-Lope, J.L. Garcia-Munoz, and M.T. Fernandez-Diaz, J. Phys.: Condends. Matter. **12**, 1361 (2000).
[12] J. Hemberger, M. Brando, R. Wehn, V. Yu. Ivanov, A.A. Mukhin, A.M. Balbashov, and A. Loidl, Phys. Rev. B **69**, 064418 (2004).
[13] E. N. Maslen, V. A. Streltsov, and N. Ishizawa, Acta Crystallogr. Sect. B **52**, 406 (1996).
[14] J.-H. Lee, Y. K. Jeong, J. H. Park, M.A. Oak, H.M. Jang, J. Y. Son, and J.F. Scott, Phys.Rev. Lett. **107**, 117201 (2011).
[15] Y.K. Jeong, J.-H. Lee, S.-J. Ahn, H.M. Jang, Solid State Communications (2012), http://dx.doi.org/10.1016/j.ssc.2012.04.010
[16] A. Revcolevschi and R. Collongues, C.R. Séances Acad. Sci., Ser. A **266**, 1797 (1969); A. Revcolevschi, Rev. Int. Htes. Temps. **7**, 73 (1970).
[17] S. Rosenkranz, M. Medarde, F. Fauth, J. Mesot, M. Zolliker, A. Furrer, U. Staub, P. Lacorre, R. Osborn, R.S. Eccleston, and V. Trounov, Phys. Rev. B **60**, 14857 (1999).